JOM, Vol. 71, No. 6, 2019
https://doi.org/10.1007/s11837-019-03459-y




# A Comparative Study on the Effect of Four-Source Ultrasonic Power on the Microstructure and Mechanical Properties of Large-Scale 2219 Aluminum Ingots

LI ZHANG,[1,2,3] RUIQING LI,[1,2,4] RIPENG JIANG,[1,2,5] LIHUA ZHANG,[1,2,3] and XIAOQIAN LI[1,2,3]

1.—Research Institute of Light Alloy, Central South University, Changsha 410083, China. 2.—State Key Laboratory of High Performance Complex Manufacturing, Changsha 410083, China. 3.—School of Mechanical and Electrical Engineering, Central South University, Changsha 410083, China. 4.—e-mail: liruiqing@csu.edu.cn. 5.—e-mail: jiangripeng@163.com

High-intensity ultrasound was introduced into the direct chill casting of large-scale 2219 aluminum alloy ingots (1380 mm in diameter and 4600 mm in length). The effects of four-source ultrasonic irradiation with various powers on the morphologies, size of α-Al grains and $Al_2Cu$ precipitated phase as well as the mechanical properties of the ingots were compared. The results indicated that, when the total real-time power of the ultrasonic system was maintained at 4030 W, a grain-refined structure with a more uniformly dispersed $Al_2Cu$ precipitated phase was obtained in the ingot. The mechanical properties of the ingot cast under a total power of 4030 W was also better than the ingots cast under 3600 W and 4420 W. It was found that the stress concentration caused by large area of coarse $Al_2Cu$ phase in the ingots under 3600 W and 4420 W resulted in the deterioration of mechanical properties.

## INTRODUCTION

Aluminum alloys have been very important in aerospace manufacturing since the introduction of metal-skinned aircraft.[1] Among all the aluminum alloys, the 2219 alloy, especially processed for high fracture toughness, is weldable and resistant to stress corrosion cracking. Therefore, it is widely used as the supersonic aircraft skin and structural members. The Space Shuttle Standard Weight Tank is also fabricated from the 2219 alloy.[2,3] For further processing into aerospace components, the 2219 aluminum alloy is usually cast into a suitable shape, usually a large-scale cylindrical ingot, and finally made into products after undergoing forging and rolling. Hence, the casting process is one of the key procedures impacting the final microstructure and performance of 2219 aluminum alloy ingots. In recent years, researchers have applied many techniques during the casting process, including chemical methods, such as adding nucleating agents, and physical methods, such as mechanical stirring, electromagnetic stirring and ultrasonic vibration. Among these methods, ultrasonic treatment (UT) has been proven to have a great potential for its high efficiency in refining the solidification structure and modifying the mechanical performance.[4,5]

Eskin[6] found that ultrasonic treatment in the developed cavitation mode is one of the effective means in the formation of non-dendritic grains in castings and billets from light alloys. El-Aziz et al.[7] investigated the effect of high-intensity ultrasonic treatment on the microstructure, corrosion and mechanical behavior of AC7A aluminum alloy. The results showed that the fine and globular aluminum grains and intermetallic particles were obtained by ultrasonic treatment during solidification. A significant improvement in corrosion attack was also noticed for the ultrasonic-treated sample. Zhang et al.[8] studied the impact of ultrasonic power and casting speed on the solidification structure of a 7050 aluminum alloy ingot in the ultrasonic field. It was found that the solidification structure of 7050 aluminum alloy melt was obviously refined and its distribution was more homogeneous after introducing the ultrasonic field in the process of semi-continuous casting. Zhong et al.[9] investigated the influence of ultrasonic vibration on the iron-

(Published online April 5, 2019)

containing intermetallic compounds of a high silicon aluminum alloy with 2% Fe. The results indicated that the finest $\delta$-$Al_4FeSi_2$ particles and only a small amount of $\beta$-$Al_5FeSi$ phase were obtained in the matrix of the Fe-containing alloy with UT for 120 s. In general, the main mechanisms put forward in the literature to explain the role of UT in grain refinement of alloys can be classified as cavitation and acoustic streaming.

However, most of the previous studies focused on the effect of a single ultrasonic system on a small-size ingot cast in the laboratory, and little attention has been paid to large-scale ingots, especially for ingots with a diameter larger than 1000 mm. This study has given an insight into the effect of the ultrasonic power of high-intensity four-source ultrasonic irradiation on the microstructure and mechanical performance of a large-scale ingot. In order to find out the best combination of ultrasonic power, a four-source ultrasonic system with three groups of power combination was employed during the solidification of a large-scale 2219 Al ingot. The microstructures of the $\alpha$-Al grains and $\theta$-$Al_2Cu$ precipitated phase in the three ingots cast under different power were compared by optical microscopy and SEM analyses. The mechanical properties of the three ingots were also examined.

## EXPERIMENTAL

### Casting Procedures

A schematic diagram of the ultrasonic system, the deployment of four sonotrodes, a typical industry-level casting scene and the real-time ultrasonic power combinations of three regimes are shown in Fig. 1. The single ultrasonic system was constituted by an ultrasonic generator with a maximum output power of 2 kW, an ultrasonic vibrator consisting of a 20-kHz piezoelectric transducer with an air cooler, an ultrasonic amplitude transformer, and a titanium acoustic sonotrode with a tip diameter of 50 mm. The chemical composition of the sonotrode is consistent with that used in our previous works.[10,11] With regard to the four-source ultrasonic system, it was composed of four ultrasonic generators and four ultrasonic vibrators, and every vibrator was controlled by an individual generator. Especially, the sonotrodes were preheated before being immersed into the melt to avoid the shock chilling of the melt. As the sonotrodes were inserted into the melt, the parameters of the generator were adjusted to ensure that the vibration reached a steady state. During ultrasonic casting, all the sonotrodes were immersed 200 mm below the melt surface in the liquid region. According to previous research,[11] the cavitation effect can reach the mushy zone and directly influence the growing microstructures. In addition, the ultrasonic-generated acoustic streaming can affect the whole large-scale melt.

Before casting, the raw materials were melted in a melting system with a protective atmosphere of argon, followed by removing the dross, stirring, degassing and filtering. Combined with the spinning nozzle inert gas flotation (SNIF®) method and a fumeless inline degassing (FILD®) method were applied to refine the melts. The Al alloy melts were then diverted into the ultrasound-assisted casting system along the launder. During solidification, the cooling water flowed around the crystallizer to chill and solidify the ingot. Meanwhile, water jets were continuously sprayed on the ingot surface until casting was completed. A cylindrical hot-top was applied to minimize the shrinkage involved. The schematic diagram of the casting system has been described elsewhere.[10,11] After 4 h of semi-continuous solidification, a large-scale cylindrical 2219 Al alloy (Al-6.20Cu-0.36Mn-0.11Zr-0.10V-0.10Fe-0.06 Si-0.01Mg-0.10Zn-0.05 wt.% Ti) ingot of 1380 mm in diameter and 4600 mm in length was successfully cast.

### Characterization

After homogenization treatment, metallographic samples with the dimensions of 15 × 15 × 20 mm and tensile specimens were taken from three different large-scale ingots treated with different ultrasonic power. The samples were obtained at specific positions from the circular plate, which was cut transversely from the top of the ingots with a thickness of 20 mm, as shown in Fig. 2.

All the samples were ground and polished through standard metallographic techniques. The microstructure was characterized by a scanning electron microscope (SEM; TESCAN, MIRA3 LMH/LMU) equipped with energy dispersive spectroscopy (EDS), and the EDS was used for compositional analysis of the phases in the samples. For metallography detection, all the samples were anodized using Barker's reagent (200 ml 32% $HBF_4$ in 800 ml distilled water) at 20 VDC for 60 s using a stainless-steel cathode. Then, a ZEISS optical microscope (Imager, A2m) equipped with an automated Zeiss AxioVision image analyzer was used under polarized light for microstructural investigation. Grain size was measured using a linear intercept method (ASTM 112-10) and statistical analysis of the results was performed. The schematic diagram and dimensions of the tensile test samples (GB/T 16865-2013) taken at the representative positions are described in Fig. 2, and the samples were tested by an Instron 3369 mechanical testing machine with a loading rate of 2 mm $min^{-1}$.

## RESULTS AND DISCUSSION

### Microstructure of the α-Al Phase

Figure 3a, b, and c shows the metallographic pictures at representative locations in the three ingots. The pictures were respectively taken from

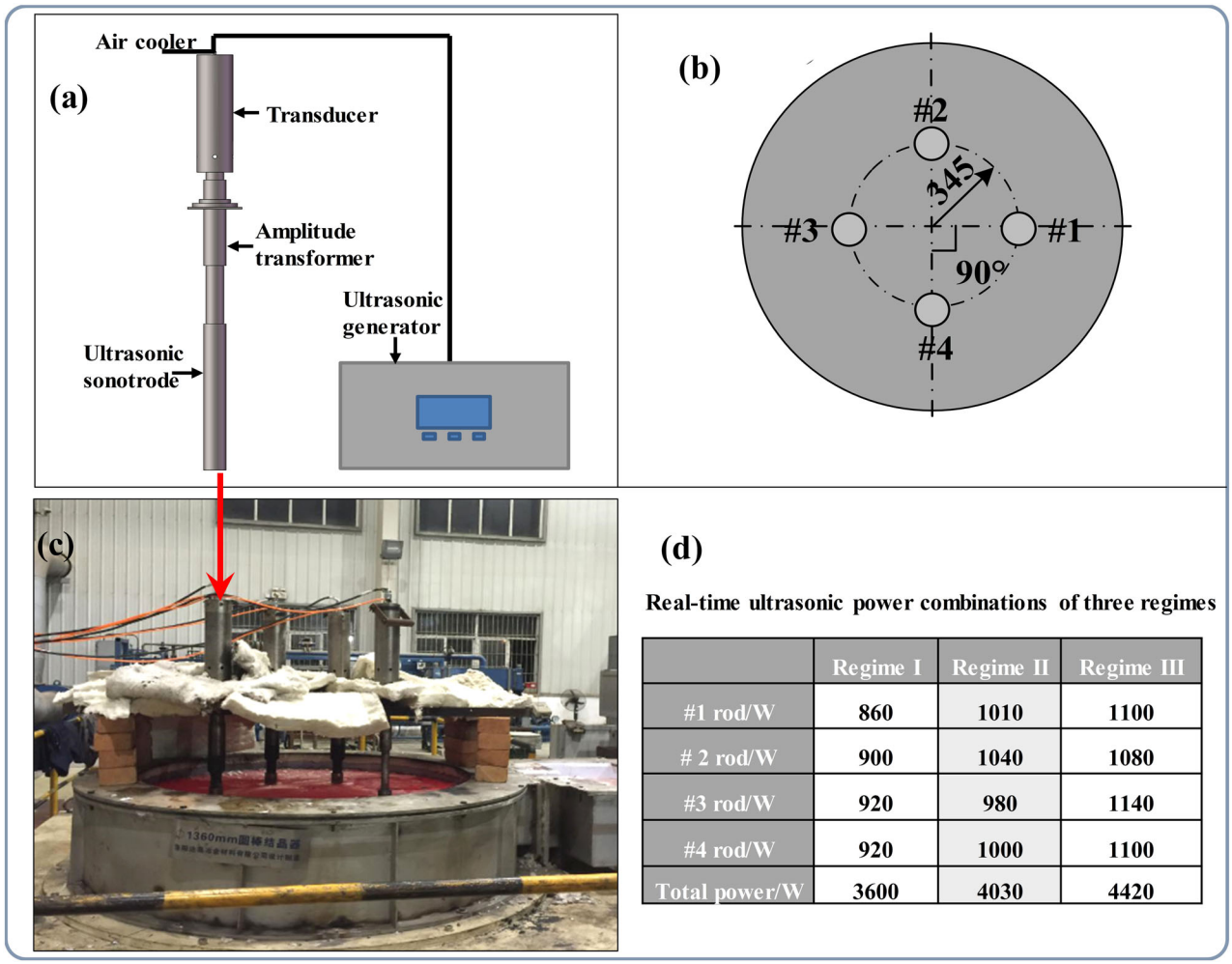


| | Regime I | Regime II | Regime III |
|---|---|---|---|
| #1 rod/W | 860 | 1010 | 1100 |
| # 2 rod/W | 900 | 1040 | 1080 |
| #3 rod/W | 920 | 980 | 1140 |
| #4 rod/W | 920 | 1000 | 1100 |
| Total power/W | 3600 | 4030 | 4420 |

Fig. 1. Schematic diagram of (a) the ultrasonic system, the deployment manners of (b) four-source sonotrodes, (c) a typical industry-level casting scene, and (d) the real-time ultrasonic power combinations of three regimes.

the center part, the half-radius and the edge part of the ingots. Dramatic differences can be seen in the size of the α-Al grains between the three different ingots. It is evident that the grain sizes of the α-Al phase at all the three sites in the ingot cast under a total ultrasonic power of 4030 W (Fig. 3b) are smaller than that in the ingots cast under 3600 W or 4420 W (Fig. 3a and c).

Figure 4 quantifies the average size of the α-Al phase at the three sites in the three ingots. Generally speaking, the average size of the α-Al grains decreases continuously from the center parts to the half-radius parts and then to the edge parts in all the three ingots. However, regarding the same sampling parts of the ingots cast under different ultrasonic powers, the average size of the α-Al grains first decreases and then increases, showing a '*V*-type' shape with the rise of the ultrasonic power. For example, the average size of the α-Al grains located at the center part is 1109.82 μm when the ingot is cast under a total ultrasonic power of 3600 W: while, with the increase of ultrasonic power to 4030 W, the average size of the α-Al grains deceases to 572.31 μm; when further increasing the ultrasonic power to 4420 W, the average size of the α-Al grains increases to 984.71 μm. In a word, when the ultrasonic power of the single rod is maintained at 1000 ± 50 W (with a total power of 4030 W), it is suitable for the four-source ultrasonic irradiation to realize the refinement of the α-Al grains in a large-scale 2219 aluminum ingot. As shown in Fig. 3a and c, compared with the ingot cast under 4030 W (Fig. 3b), the morphologies of the α-Al grains in the ingots cast under 3600 W and 4420 W are irregular even at the edge part, while the α-Al grains are regular and uniform at the edge part of the ingot cast under 4030 W. In fact, at the edge part of the ingot, the formation of equiaxed grains is mainly attributed to the high cooling rate caused by the cooling water which is sprayed directly onto this part. The cooling rate and speed of heat transfer are much lower at the center part due to the large-dimensional difference. However, the vibration of ultrasound can reduce the inter-dendritic bridging and suppress the dendritic arm growth or the fragment dendritic arm, which

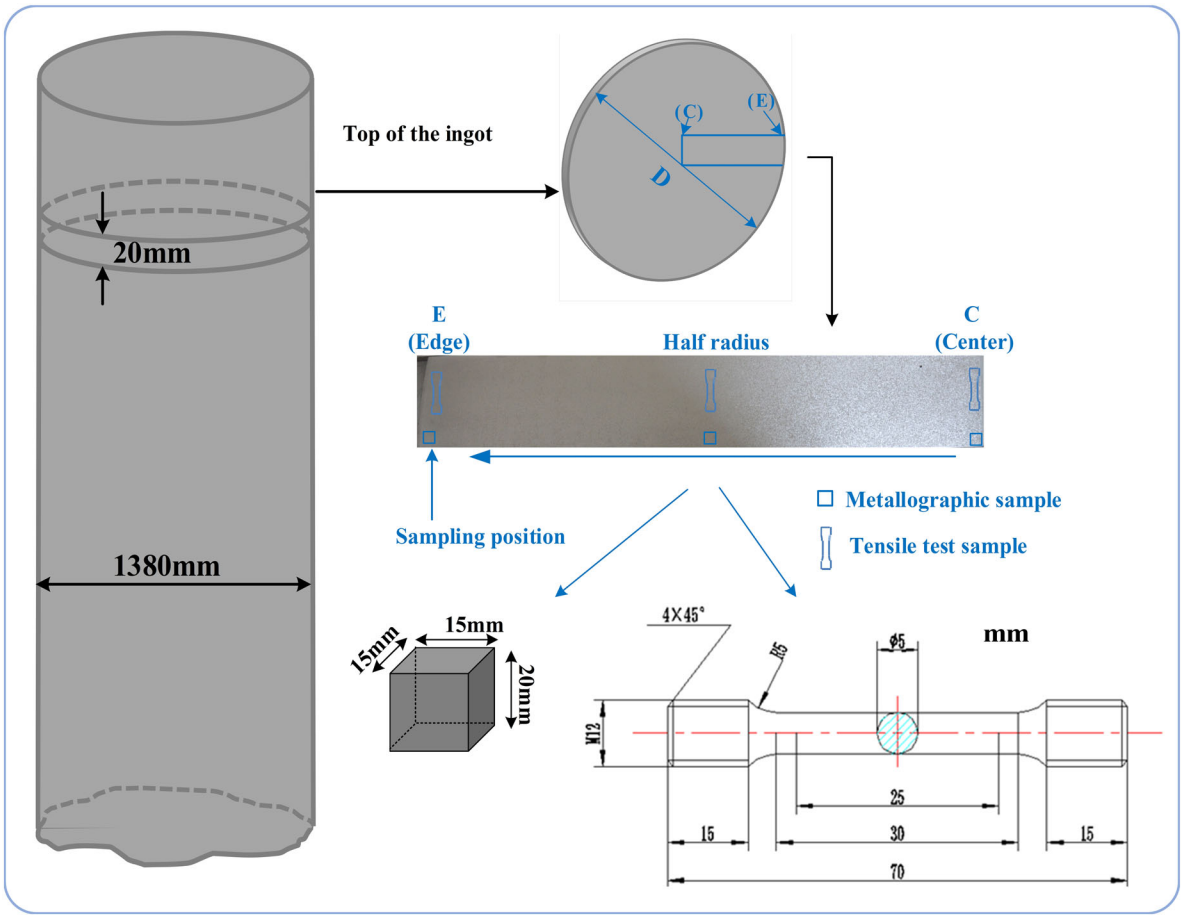


Fig. 2. Schematic diagram showing the representative positions of microstructure specimens and tensile test samples taken from the ingots.

strengthens the grain refinement.[12] The variance in the average grain size of the α-Al solidified with different ultrasonic powers indicates that the ultrasonic treatment still has a certain influence on the microstructure of the edge part.

Under ultrasonication, huge energy and microjets with a powerful impact are produced from the collapse of cavitation bubbles. The contamination of the particles' surface is reduced by the continuous microjet flow, which improves the wettability of particles acting as heterogeneous nucleation sites.[13–15] These nucleation particles may come from either in situ formation or the native potent particles that are present in melts. For instance, it has been well documented that $TiAl_3$, $ZrAl_3$, $NbAl_3$, and/or $BTi_2$ can serve as the efficient nucleation sites. As more potential nucleation particles were activated, the grain refinement of the α-Al grains is enhanced.[16–18]

It can be concluded that the power of the ultrasonic system during the solidification process has a great impact on the size and morphology of the α-Al grains. However, the refinement effect will be weakened if there is an over-increase in the power of the ultrasonic equipment during solidification. When the power of every single rod is increased to 1100 ± 50 W (with a total power of 4420 W), the refinement effect is inferior to the situation where the total power is 4030 W. Nevertheless, it is superior to the situation where the power of a single rod is decreased to 900 ± 50 W (with a total power of 3600 W). This result suggested that the power of every single rod should be maintained at 1000 ± 50 W, and that the intensity of ultrasound can effectively increase the cavitation capacity. Finally, the heat and the crystal nucleus are uniformly distributed across the ingot due to the huge energy liberated through the bursting of cavitation bubbles.

According to Gao et al. and Campbell,[19,20] the cooling rate of the melt and the acoustic streaming effect are enhanced by the increase of ultrasonic power. The cavitation and convection effect under the power of 900 ± 50 W per rod are not as powerful as that under the power of 1000 ± 50 W per rod. However, with the increase of total power to 4420 W (1100 ± 50 W per rod), the cavitation bubbles may be increased to a very large extent in the expansion phase of ultrasound, resulting in the cavitation bubbles being incapable of collapsing immediately within the compression phase.[21] Thus, a large

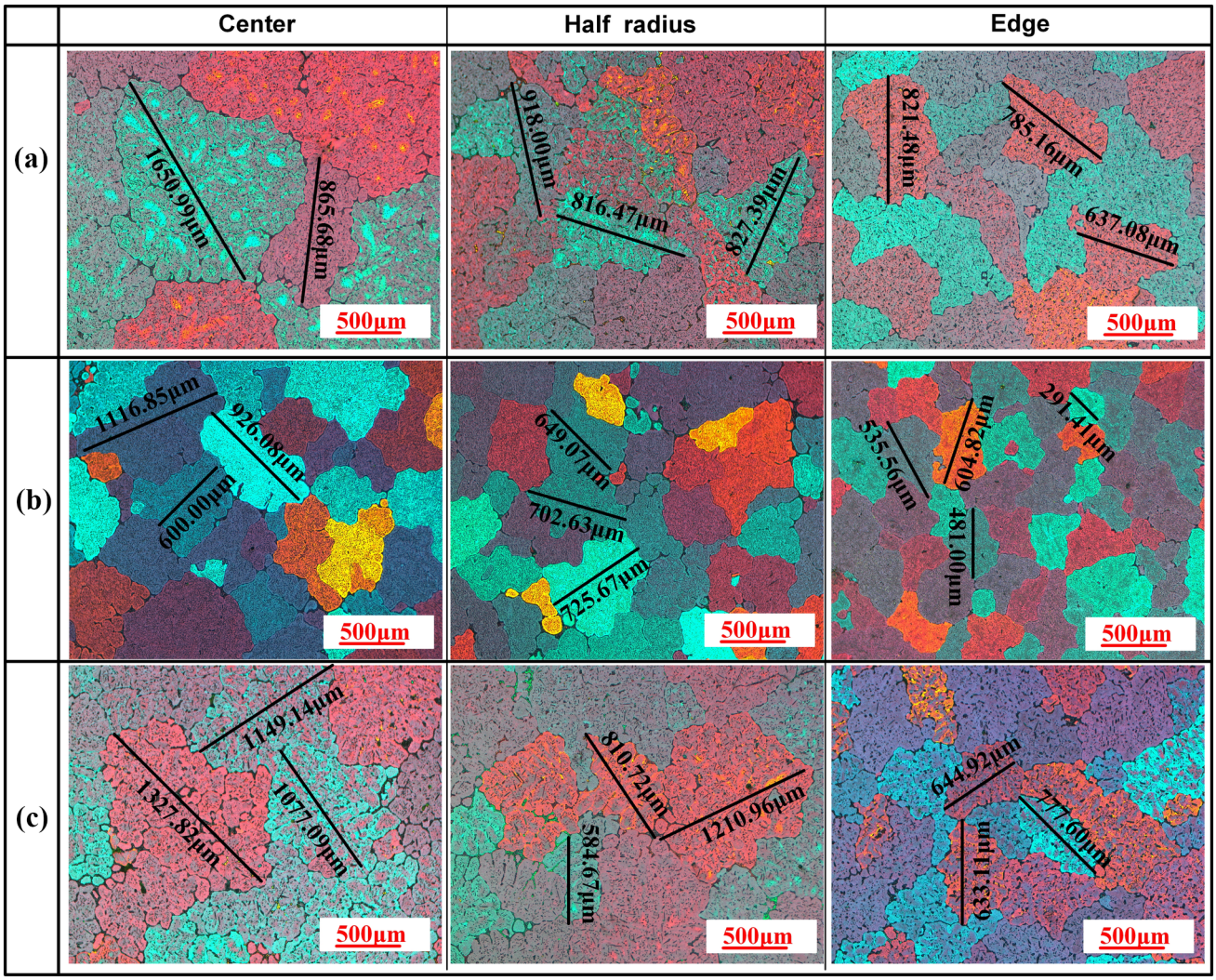


Fig. 3. Optical micrographs at center part, half-radius and the edge part of 2219 ingots under ultrasonic treatment with (a) a total power of 3600 W, (b) a total power of 4030 W and (c) a total power of 4420 W.

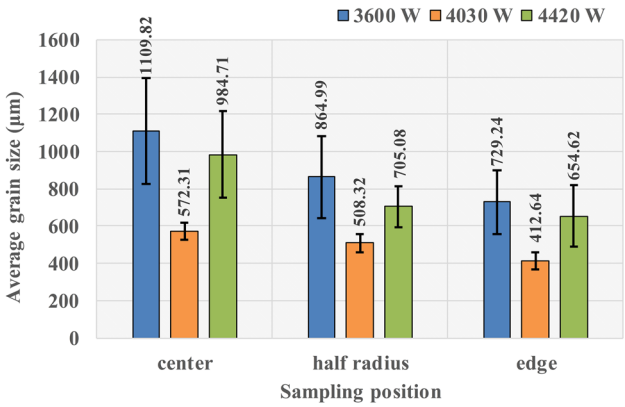


Fig. 4. The average grain size of α-Al grains at the representative positions of the ingots treated under different ultrasonic powers.

amount of useless cavitation bubbles will be generated, thereby increasing the scattering attenuation and reducing the cavitation intensity.[4,21,22] In addition, Eskin has proposed that the introduction of ultrasonic energy into the melt increases the temperature and effectively decreases the undercooling at the solidification front.[23] Fang[24] has indirectly verified this assumption that the ultrasonic power continuously increasing to 1200 W is negative for the grain refinement, and the excessive energy may be introduced and converted into heat in the Mg-3RE-3Zn-0.7Y melt.

On the other hand, the increase of power to 1100 ± 50 W per rod may cause an irregular superposition or the offset of the oscillatory wave of the ultrasound between the rods, resulting in a great difference between the vibration frequency of the ultrasound and the nucleation particles. This could weaken the liquid metal convection between the crystals and lower the stirring effect on the solidification front, which is detrimental to the heat transfer and homogenization of the nucleation particles. Further study is being performed to validate this speculation.

### Microstructure of the Precipitated Phase

Figure 5a, b, and c shows the SEM and EDS results at different positions of the three different ingots. From the EDS result presented in Fig. 5a, the precipitated phase on the grain boundaries can be inferred as the $\alpha$-Al + $\theta$-$Al_2Cu$ eutectic phase. The previous studies have demonstrated that the needle-like precipitated phases inside the grains are $\theta'$-$Al_2Cu$ or $\theta''$-$Al_2Cu$, and that the dot-like precipitated phase is $\theta$-$Al_2Cu$.[25] The morphologies and size of the precipitated phase located on the grain boundaries and inside the grains are different from the center part to the edge part in all the ingots, and there is a great difference in the structures of the precipitated phase at the same positions between the three ingots. It can be seen that massive coarse eutectic phases flock together on the grain boundaries and account for large areas at the center part in the three ingots, as shown in Fig. 5, especially in ingots cast under 3600 W and 4420 W (Fig. 5a and c). The area of the eutectic phase on the grain boundaries is obviously decreased both at the half-radius and at the edge part in the ingot cast under 4030 W (Fig. 5b). In the other two ingots, this

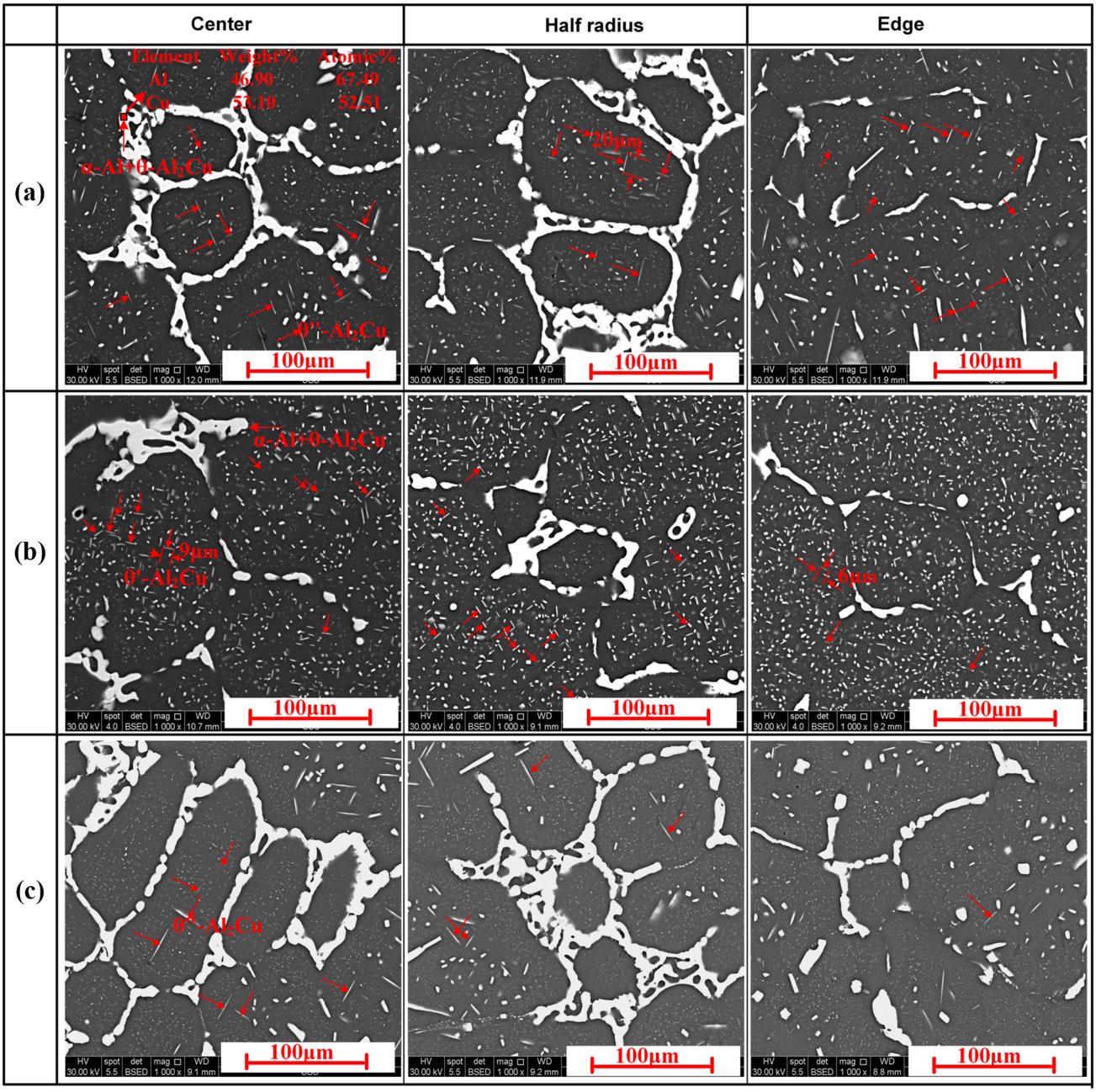


Fig. 5. SEM images of the precipitated phases at the representative positions of 2219 ingots under ultrasonic treatment with (a) a total power of 3600 W, (b) a total power of 4030 W and (c) a total power of 4420 W.

variation is only prominent at the edge part. In addition, a mass of refined dot-like $\theta$-$Al_2Cu$ are evenly distributed and there are little long needle-like $\theta'$-$Al_2Cu$ or $\theta''$-$Al_2Cu$ phase existing inside the grains across the ingot cast under 4030 W. However, most of the precipitated phase within the grains are long needle-like $\theta'$-$Al_2Cu$ or $\theta''$-$Al_2Cu$ phase and there are little dot-like $\theta$-$Al_2Cu$ phase inside the grains especially in the ingot cast under 3600 W, which can also be seen in Fig. 3a

In order to quantify the area fractions of the coarse eutectic phase on the grain boundaries and the number density (the number of particles per area in $\mu m^2$) of dot-like $\theta$-$Al_2Cu$ particles inside the grains, Image Pro Plus software was used to evaluate the two indexes. Figure 6 presents the area fraction of the coarse eutectic phases with an area $\geq 20$ $\mu m^2$ and the number density of dot-like $\theta$-$Al_2Cu$ particles with an area $< 20$ $\mu m^2$ in the three ingots. The area fraction of the coarse eutectic phase is reduced by 65.24% from the center part to the edge part (from 68.88% to 23.94%) in the ingot cast under 4030 W, while there is a marginal decrease in this value in the ingots cast under 3600 W and 4420 W. Regarding the density of dot-like $\theta$-$Al_2Cu$ particles, it is increased by 128.81% (from 5.9 to 13.5) from the center part to the edge part in the ingot cast under 4030 W, by 114.89% in the ingot cast under 3600 W, and by 49.41% in the ingot cast under 4420 W. Although this value in all three ingots is improved, the values at the half-radius and the edge part in the ingot cast under 4030 W are higher than those in the other two ingots. Thus, the primary $\alpha$-Al grains and precipitated phase are both refined by a reasonable setting of the ultrasonic power during solidification.

The refinement of the precipitated phase can be attributed to the following mechanisms: ($q$) the compulsive stirring and homogenization action resulted from acoustic streaming will distribute Cu atoms more uniformly throughout the ingot during the solidification process,[11] reducing the formation of the coarse $Al_2Cu$ phase; (2) cavitation-induced high-speed flow in the melt also helps to accelerate the heat transfer and cooling rate, suppressing the growth of the $Al_2Cu$ phase;[26] and (3) the grain boundaries of the $\alpha$-Al phase became discontinuous and thinner in the ingot cast under 4030 W, which resulted in the formation of a thinner and smaller scattered precipitated phase on the grain boundaries. In addition, the refined $\alpha$-Al grains produce more grain boundaries, which in turn reduce the interface energy, resulting in precipitation of the eutectic phase in more locations.[26] Thus, the agglomeration of the coarse eutectic phase on the grain boundaries is suppressed and thereby the continuity is decreased.

## Mechanical Properties

The mechanical properties of the samples are shown in Fig. 7a, b, and c. It can be seen clearly that the mechanical properties of ingot cast under 4030 W are better than the other two ingots in all the sampling positions. In addition, the mechanical properties at the edge part of the ingots are superior to those at the center part and at half-radius, especially in the ingot cast under 4030 W. When the power of every single rod is maintained at $1000 \pm 50$ W, the ultimate tensile strength is improved by 13.9%, from 180.18 MPa (center part) to 205.25 MPa (edge part), and meanwhile the elongation is increased by 204.40% from 4.73% (center part) to 14.40% (edge part).

According to the Hall–Petch formula: $\sigma_s = \sigma_0 + Kd^{-1/2}$ ($\sigma_0$ is a material constant, $K$ is the Hall–Petch slope, and $d$ is the average grain size), the strength of a material is negatively correlated with the grain size.[27] Hence, the mechanical properties of the ingots with finer grains are better. However, the refinement of the primary $\alpha$-Al grains is not the simple reason giving rise to the enhancement of the mechanical properties of the large-scale 2219 aluminum ingots. Aghayani et al.[26] demonstrated that

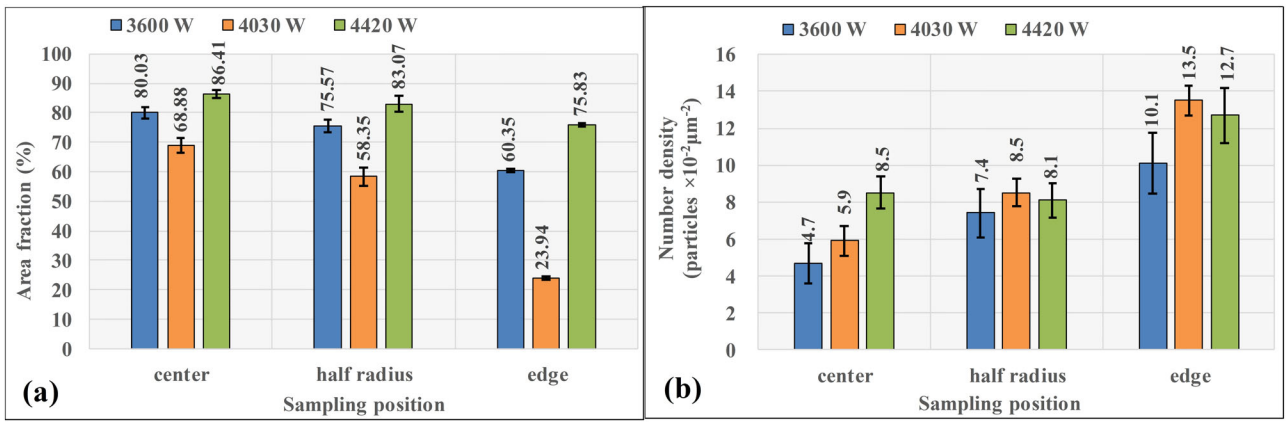


Fig. 6. (a) The area fraction of the precipitated phases with areas more than 20 $\mu m^2$ and (b) the number density of the precipitated particles with areas less than 20 $\mu m^2$ at representative positions of 2219 ingots treated under different ultrasonic power.

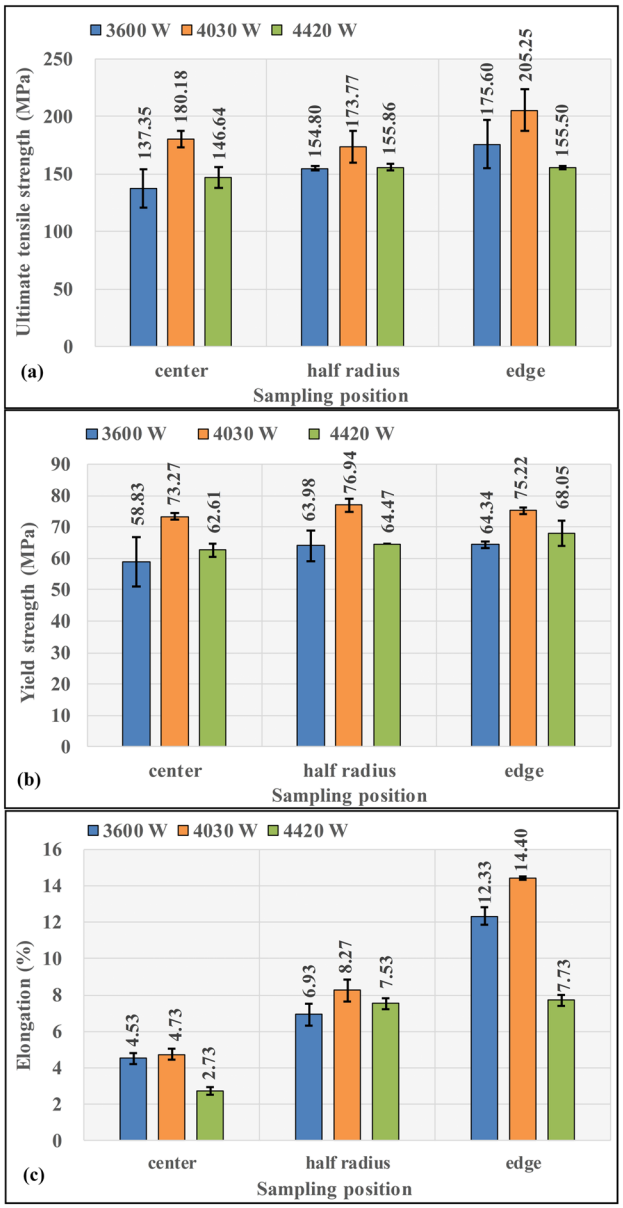


Fig. 7. (a) The ultimate tensile strength at the specific positions, (b) the yield strength at the specific positions and (c) the elongation at the specific positions of the 2219 ingots treated under different ultrasonic powers.

evenly distributed intermetallic particles can promote the mechanical properties of AZ91 magnesium alloy. Thus, the uniformly dispersed dot-like $\theta$-$Al_2Cu$ phase inside the $\alpha$-Al grains can also promote the mechanical properties of large-scale ingots. In general, the refined primary $\alpha$-Al grains and the evenly distributed tiny $\theta$-$Al_2Cu$ particles inside the grains together improve the mechanical performance of the large-scale ingot cast under 4030 W.

Figure 8 shows the micro-fracture morphology of the specimens at the edge part of the three ingots after tensile testing. It can be seen that many transgranular fractures (rough surface indicated by red lines) exist in the ingots, especially in the ingots cast under 3600 W and 4420 W, while most of the fracture area in the ingot cast under 4030 W are intergranular fractures. The surface of the transgranular fracture is covered with a large chunk of coarse $Al_2Cu$ phase and large $Al_2Cu$ particles (indicated by the red circles) can be seen in the shallow dimples in the ingot cast under 4420 W. The occurrence of the intergranular fracture might result from the stress concentration caused by the precipitation of the coarse $\theta$-$Al_2Cu$ phase on the grain boundaries.[28] The smoother fracture surface in the ingot cast under 4030 W indicates that fewer coarse $Al_2Cu$ phase flock together on the grain boundaries, which is consistent with the statistical results shown in Fig. 6a. The stress concentration is decreased owing to the reduction of the coarse $Al_2Cu$ phase and therefore this improves the intracrystalline plasticity and mechanical strength.

## CONCLUSION

In this study, the effects of four-source ultrasonic systems with different powers on the morphologies, the size of the $\alpha$-Al grains and the $Al_2Cu$ precipitated phase, as well as the mechanical properties of the large-scale 2219 aluminum ingots were compared. The main conclusions can be summarized as follows:

(1) The power of the ultrasonic system had a great effect on the morphologies of the $\alpha$-Al grains and the $Al_2Cu$ precipitated phase. Compared with the ultrasonic treatment under a total power of 3600 W (with a single power of 900 $\pm$ 50 W) and 4420 W (with a single power of 1100 $\pm$ 50 W), the ultrasonic system under a total power of 4030 W (with a single power of 1000 $\pm$ 50 W) had a more effective impact on refining the $\alpha$-Al grains and the precipitated $Al_2Cu$ phase. Coarse $\alpha$-Al grains are predominant in the center part of the ingots, and the size was decreased dramatically in the edge part, especially in the ingot cast under 4030 W. The area fraction of the coarse $\theta$-$Al_2Cu$ phase precipitated on the grain boundaries in the ingot cast under 4030 W was much lower than that in the ingots cast under 3600 W and 4420 W. At the power of 4030 W, the area fraction of the coarse precipitated phase was reduced by 65.20% and the number density of dot-like $\theta$-$Al_2Cu$ particles inside the grains was increased by 128.81% from the center to the edge part.

(2) The ultimate tensile strength, yield strength and elongation at all the sampling positions in the ingot treated under 4030 W were higher than those under 3600 W or 4420 W, and the mechanical properties were improved from the center part to the edge part in all the ingots. The mechanical properties were closely related to the distribution and size of the $\alpha$-Al grains and the $\theta$-$Al_2Cu$ phase. The $\theta$-$Al_2Cu$

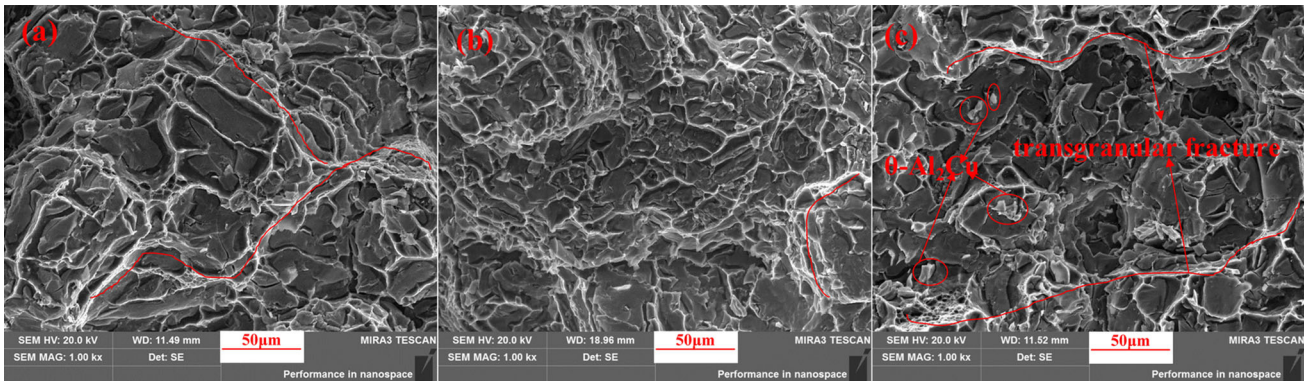


Fig. 8. SEM images of the tensile fracture surfaces in ingots cast under a total ultrasonic power of (a) 3600 W, (b) 4030 W and (c) 4420 W.

precipitated phase on the grain boundaries and inside the grains in the ingot cast under 4030 W were both refined. Finally, the refined primary $\alpha$-Al grains and the evenly distributed tiny $\theta$-$Al_2Cu$ particles inside the grains together improved the mechanical properties of the large-scale ingot cast under 4030 W.

## ACKNOWLEDGEMENTS

This work was supported by the National Natural Science Foundation of China (Grant No. U1637601, No. 51475480, No. 51575539), the State Key Laboratory of High Performance Complex Manufacturing of Central South University (Contract No. ZZYJKT2017-01) and the Project of Innovation-driven Plan for Postgraduate in Central South University (No. 2017zzts104).

## REFERENCES

1. I.J. Polmear, *Light Alloys*, 3rd ed. (London: Arnold, 1995), p. 250.
2. R.S. Shevell, *Fundamentals of Flight*, 2nd ed. (Englewood Cliffs: Prentice Hall, 1989), pp. 120–319.
3. W.O. Soboyejo and T.S. Srivatsan, *Advanced Structural Materials: Properties, Design Optimization, and Applications*, 1st ed. (Boca Raton: CRC, 2006).
4. G.I. Eskin and D.G. Eskin, *Ultrasonic Treatment of Light Alloy Melts*, 2nd ed. (Boca Raton: CRC, 2014).
5. O.V. Abramov, *High-Intensity Ultrasonics: Theory and Industrial Applications*, 1st ed. (Boca Raton: CRC, 1999), pp. 200–217.
6. G.I. Eskin, *Z. Metallkd.* 93, 502 (2002).
7. A.M. El-Aziz, M.A. El-Hady, and W. Khlifa, *Light Metals*, ed. E. Williams (New York: Springer, 2016), p. 721.
8. L.H. Zhang, J. Yu, X.M. Zhang, and J. Cent, *South Univ.* 17, 431 (2010).
9. G. Zhong, S.S. Wu, H.W. Jiang, and A. Pan, *J. Alloys Compd.* 492, 482 (2010).
10. R.Q. Li, Z.L. Liu, P.H. Chen, Z.T. Zhong, and X.Q. Li, *Adv. Eng. Mater.* 19, 1600375 (2017).
11. R.Q. Li, Z.L. Liu, F. Dong, X.Q. Li, and P.H. Chen, *Metall. Mater. Trans. A* 47, 3790 (2016).
12. V.M. Sreekumar and D.G. Eskin, *JOM* 68, 3088 (2016).
13. O. Kudryashova and S. Vorozhtsov, *JOM* 68, 1307 (2016).
14. H.R. Kotadia, M. Qian, D.G. Eskin, and A. Das, *Mater. Des.* 132, 266 (2017).
15. G. Wang, M.S. Dargusch, M. Qian, D.G. Eskin, and D.H. StJohn, *J. Cryst. Growth* 408, 119 (2014).
16. L. Zhang, D.G. Eskin, and L. Katgerman, *J. Mater. Sci.* 46, 5252 (2011).
17. F. Wang, Z.L. Liu, D. Qiu, J.A. Taylor, and M.X. Zhang, *Acta Mater.* 61, 360 (2013).
18. F. Wang, Z.L. Liu, D. Qiu, J.A. Taylor, and M.X. Zhang, *J. Appl. Cryst.* 47, 770 (2014).
19. D.M. Gao, Z.J. Li, Q.Y. Han, and Q.J. Zhai, *Mater. Sci. Eng. A* 502, 2 (2009).
20. J. Campbell, *Int. Met. Rev.* 26, 71 (1981).
21. B.E. Noltingk and E.A. Neppiras, *Proc. Phys. Soc. Lond. B* 63, 647 (1950).
22. L. Rayleigh, *Philos. Mag.* 34, 941 (1917).
23. G.I. Eskin and D.G. Eskin, *Ultrason. Sonochem.* 10, 297 (2003).
24. X.G. Fang, S.S. Wu, Z. Li, S.L. Lü, and P. An, *Rare Met. Mater. Eng.* 45, 7 (2016).
25. X.B. Liu, Y. Osawa, S. Takamori, and T. Mukai, *Mater. Lett.* 62, 2872 (2008).
26. M.K. Aghayani and B. Niroumand, *J. Alloys Compd.* 509, 114 (2011).
27. J.W. Kang, X.F. Sun, K.K. Deng, F.J. Xu, X. Zhang, and Y. Bai, *Mater. Sci. Eng. A* 697, 211 (2017).
28. G.M. Ludtka and D.E. Laughlin, *Metall. Trans. A* 13, 411 (1982).